



Chemical order and local structure of the lead-free relaxor ferroelectric $\text{Na}_{1/2}\text{Bi}_{1/2}\text{TiO}_3$

Melanie Gröting*, Silke Hayn, Karsten Albe

Fachgebiet Materialmodellierung, Institut für Materialwissenschaft, TU Darmstadt, Petersenstr. 32, 64287 Darmstadt, Germany

ARTICLE INFO

Article history:

Received 25 March 2011

Received in revised form

18 May 2011

Accepted 29 May 2011

Available online 6 June 2011

Keywords:

Perovskite

Relaxor

NBT

Chemical order

Local structure

ABSTRACT

The A-site mixed perovskite sodium bismuth titanate ($\text{Na}_{1/2}\text{Bi}_{1/2}\text{TiO}_3$) (NBT) is investigated by means of first-principles calculations based on density functional theory. By studying different geometries with varying occupations of the A-site, the influence of chemical order on the thermodynamic stability and local structure is explored. We find that the hybridization of Bi 6sp with O 2p-states leads to stereochemically active Bi^{3+} lone pairs and increases the stability of structures with high Bi concentrations in {001}-planes. This goes along with displacive disorder on the oxygen sublattice, which up to now has been neglected in experimental studies. The calculated ordering energies are, however, small as compared to the thermal energy and therefore only short-range chemical order can be expected in experiments. Thus, it is conceivable that chemically ordered local areas can act as nucleation sites for polar nano-regions, which would explain the experimentally observed relaxor behavior of NBT.

© 2011 Elsevier Inc. All rights reserved.

1. Introduction

The mixed perovskite ($\text{Na}_{1/2}\text{Bi}_{1/2}\text{TiO}_3$) (NBT) is one rare example of A-site mixed relaxor ferroelectrics. NBT-based materials show extraordinarily high strains and are promising environmentally friendly alternatives to the toxic lead-containing standard material in piezoelectric applications $\text{Pb}(\text{Zr},\text{Ti})\text{O}_3$ (PZT). Additionally, the fact that Bi^{3+} is iso-electronic to Pb^{2+} , both exhibiting a lone pair effect, has encouraged further studies on structural, chemical and electrical properties of this material by both experimental and theoretical methods [1–20]. Pure NBT ceramics show strong ferroelectric properties with large remanent polarization [1], but they are difficult to pole due to their high coercive field and conductivity caused by oxygen vacancies [2]. For overcoming these problems NBT-based solid solutions have been studied. Especially, recent results on ($\text{Na}_{1/2}\text{Bi}_{1/2}\text{TiO}_3$ – BaTiO_3 –($\text{K}_{1/2}\text{Na}_{1/2}\text{NbO}_3$) (NBT–BT–KNN) solid solutions revealed promising piezoelectric properties [3,21].

After Smolenskii discovered NBT in 1960 [4], structural, vibrational and dielectric properties have been investigated in detail [1,3,5–17]. Neutron powder diffraction studies showed that NBT above 540 °C is in its cubic prototype phase (space group $Pm\bar{3}m$). On cooling it undergoes two reversible phase transformations. Between 400 and 500 °C a tetragonal structure with space group

symmetry $P4bm$ exists with in-phase $a^+a^+c^+$ octahedral tilting and anti-parallel cation displacements along [001], the tetragonal distortion from cubic is rather small with 0.14% [5,6]. Below 255 °C a rhombohedral $R3c$ structure is stable with anti-phase $a^-a^-a^-$ octahedral tilting and ion displacements along the [111]-direction of the pseudo-cubic cell with $\alpha = 89.83^\circ$ [6]. High-resolution single-crystal X-ray diffraction revealed that there might exist monoclinic-like deviations from $R3c$ -symmetry [7], local deviations from the average structure were also subject of an earlier work of Thomas et al. [8]. Recently, an additional intermediate orthorhombic phase in the temperature range 280–320 °C having $Pnma$ -symmetry and $a^-b^+a^-$ octahedral tilting bridging the rhombohedral and tetragonal phase was found by TEM and electron diffraction [9,10]. Already at 200 °C $Pnma$ -modulation of the $R3c$ -phase starts, which can be understood as formation of twin planes with $Pnma$ -symmetry within the $R3c$ -host. The same authors refined the tetragonal phase above 400 °C in the centrosymmetric space group $P4/mbm$, the phase transition from $Pnma$ to $P4/mbm$ occurs between 320 and 370 °C. All these information are summarized in Fig. 1.

In the temperature range of the diffuse phase transition from the rhombohedral to the tetragonal phase (200–320 °C), NBT exhibits peculiar antiferroelectric [11], relaxor-like behavior [1] with electric field-induced phase transitions [3,12].

The origin of the relaxor behavior is still controversial, but in B-site mixed perovskites it is associated with heterovalent disorder [22,23]. NBT has aliovalent cations on the A-site (Na^+ and Bi^{3+}) in the exact ratio 1:1. For B-site mixed perovskites chemical

* Corresponding author.

E-mail addresses: groeting@mm.tu-darmstadt.de (M. Gröting), shayn@mm.tu-darmstadt.de (S. Hayn), albe@mm.tu-darmstadt.de (K. Albe).

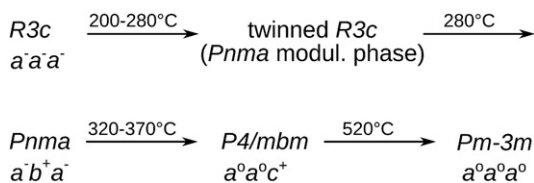


Fig. 1. Phase transitions of NBT with variation in temperature.

ordering is generally understood [24]. Order, commonly rock salt (111)-order, occurs when the charge difference between the cation species occupying the same crystallographic site is $\Delta q > 2$, while for charge differences $\Delta q < 2$ disorder is found. For $\Delta q = 2$ disordered, partially ordered and fully ordered examples can be found depending on size and/or bonding preferences of the different cations. In contrast, A-site ordering is much less common. There exist only a few examples where A-site order is experimentally found. Knapp and Woodward reported on (001)-order for $(\text{Na}_{1/2}\text{La}_{1/2})(\text{Mg}_{1/2}\text{W}_{1/2})\text{O}_3$ driven by cooperative effects of both A-site and B-site ordering [25]. More examples can be found in a review recently published by King and Woodward [26]. They show that A-site order commonly occurs in {001}-layers, but that charge differences between the cations of $\Delta q = 2$ are not sufficient to cause ordering. Systematic oxygen vacancies, vacancies in the A-sublattice or B-site ordering are necessary to stabilize chemical A-site order in mixed perovskites.

Nonetheless, many authors reported on chemical order in NBT. Park suggested a low degree of Bi/Na-order in NBT with an ordered face-centered structure (space group $Fm\bar{3}m$) for the high-temperature cubic phase based on single-crystal XRD measurements [13]. Dorcet and Trolliard recently proposed the same type of order based on TEM images and electron diffraction. According to them ordering occurs in nanometer sized domains embedded in a disordered matrix [10]. Rock salt type order was also deduced from Raman spectra, which indicated an additional strong lattice disorder [14]. Chemical short-range order emerging as segregation planes with correlated cation displacements along $\langle 001 \rangle$ (comparable to Guinier-Preston-Zones in metal alloys) leading to asymmetric streak patterns in diffuse scattering was suggested by Kreisel et al. [15]. Besides these streaks Thomas et al. [16] could identify additional satellite reflections in their reciprocal space maps which are thought to have their origin in a modulated domain structure. Structural polar disorder of the Bi-sites is assumed by Shuvaeva et al. to explain XAFS results [17]. They find that statistically disordered Bi-displacements deviating from the [111]-direction lead to few short Bi-O bonds of 2.22 Å. However, this short bond length never appeared in average crystal structures deduced from diffraction methods implying that strong local disorder exists in NBT due to the mixed cationic A-site.

Theoretical methods, in contrast, have only scarcely been used for studying this material. Xu and Ching investigated the electronic structure of pure NBT and its solid solution with BaTiO_3 by means of an orthogonalized linear combination of atomic orbitals (OLCAO) method, but they only considered the rock salt type of chemical order and did not include structural relaxations [18]. Burton and Cockayne conducted a cluster expansion-supported search on the ground state structure of NBT based on *ab initio*-calculations [19]. They predicted a monoclinic structure (space group Pm , unique c -axis) within a 40-atom supercell with “criss-cross” rows of Na and Bi perpendicular to [001] (cf. 10-01_z configuration in Fig. 2 for cation order). In our recent study, we compared first-principles calculations and TEM images of the solid solution of NBT and BaTiO_3 within the composition range of the morphotropic phase boundary, showing that in this material

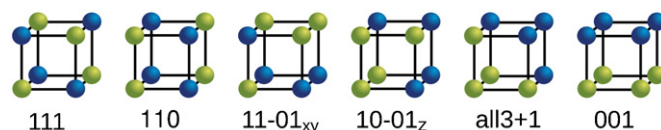


Fig. 2. $2 \times 2 \times 2$ perovskite supercell configurations, the simple cubic sublattice of A-atoms is only shown (Bi: green, Na: blue). (For interpretation of the references to color in this figure legend, the reader is referred to the web version of this article.)

the distribution of Ba/Bi/Na is homogeneous, hence no distinctive chemical order occurs [20].

With respect to the massive discrepancies between general empirical models, experimental and theoretical work, it thus appears to be a worthwhile task to revisit the problem of chemical order in NBT.

In order to gain insights into the chemical ordering tendency and the consequences for the local structure we investigated six different cation configurations in $2 \times 2 \times 2$ (pseudo)cubic perovskite supercells using total energy calculations based on electronic density functional theory [27,28].

We present total energies and densities of states of these configurations in structurally relaxed configurations. Regarding the tendency for chemical ordering we discuss the observed total energy differences in the light of thermodynamics by comparing the values with mixing energies at elevated temperatures. We analyze the local structure induced by the different cation orders and identify the driving forces for the observed atomic displacements by discussing selected densities of states.

In doing so, we focus on the high-temperature cubic phase, where mobility is sufficiently high to allow for cation redistribution. However, the displacive disorder on the oxygen sublattice induced by cation order is also relevant for the low temperature phases of NBT, because the chemical order installed at high temperatures will be frozen in.

2. Method

The Vienna Ab-initio Simulation Package (VASP) [29–32] was used to perform fully relaxed total energy calculations. Projector Augmented Plane Waves [33,34] were applied with the LDA exchange correlation functional [35]. An $8 \times 8 \times 8$ Monkhorst-Pack k -point mesh for the primitive cell was used for Brillouin zone integration [36]. In all calculations, the plane-wave energy cutoff was set to 750 eV resulting in a numerical error of less than 1 meV/atom.

The valence electron configurations of the PAW data sets were: Bi $5d^{10}6s^26p^3$, Na $2p^63s^1$, Ti $3s^23p^64s^23d^2$ and O $2s^22p^4$.







Calculations were performed with relaxation of atomic positions at the experimental cell volume (lattice constant $a=3.9137$ Å). Forces were optimized to less than 0.005 eV/Å.

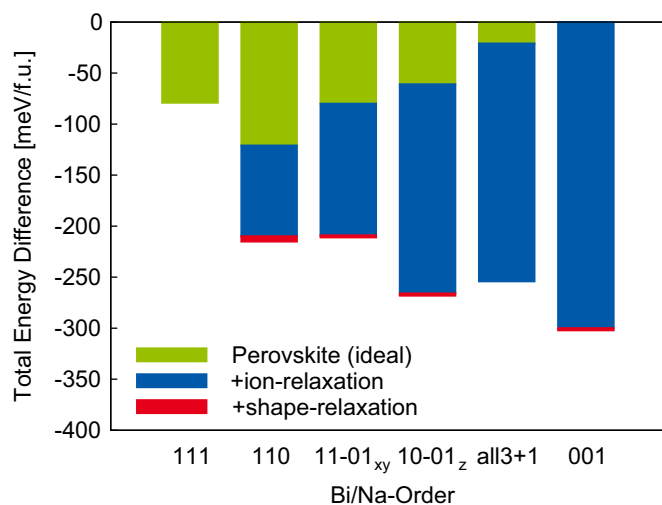
Additional calculations with the PBE exchange correlation functional [37] lead to the same conclusions.

In a $2 \times 2 \times 2$ perovskite supercell there are eight A-atoms on a simple cubic sublattice. For a 1:1 composition there exist six distinctive arrangements of A-atoms, the resulting configurations are shown in Fig. 2. Three of these configurations correspond to layered structures along the three high-symmetry (pseudo)cubic directions [001], [110] and [111]. In ‘10-01_z’ and ‘11-01_{xy}’, there are only columns of same cations present. In the ‘10-01_z’ configuration these columns are arranged along [10(0)]- and [01(0)]-directions alternately stacked along the z -axis, while in the ‘11-01_{xy}’ configuration they are arranged along [(0)11]- and [(0)01]-directions when looking along the x -axis and along

Table 1

Properties of the relaxed structures of different Bi/Na-configurations. Also shown are the occurrences of different oxygen coordinations, and bandgaps are given.

A-site configuration	111	110	11-01 _{xy}	10-01 _z	all3+1	001
Space group	$Fm\bar{3}m$	$P4/mmm$	$P4/mmm$	$P4_2/mmc$	$Pm\bar{3}m$	$P4/mmm$
Relaxed structures						
c/a-ratio	1.000	0.989	1.002	1.003	1.000	1.001
Ti displacement (Å)	0.00	0.00	0.02	0.02	0.03	0.04
O displacement (Å)	0.00	0.09	0.15	0.14	0.13	0.16
Oxygen coordination						
 4 × Na						1/6
 4 × Bi						1/6
 1 × Bi/3 × Na			1/6	1/3	1/2	
 3 × Bi/1 × Na			1/6	1/3	1/2	
 2 × Bi/2 × Na (cis)		2/3	1/3	1/3		2/3
 2 × Bi/2 × Na (trans)	6/6	1/3	1/3			
Bandgap (eV)	1.50	1.87	1.80	2.01	1.94	1.90

**Fig. 3.** Total energies from DFT calculations in ideal perovskite (green) and relaxed structures (blue and red). The total energy of the ideal perovskite '001' is set to zero. Energy changes from cell shape relaxation (red) are very small. (For interpretation of the references to color in this figure legend, the reader is referred to the web version of this article.)

[1(0)1]- and [0(0)1]-directions when looking along the *y*-axis. The 'all3+1' configuration is characterized by the fact that in adjacent {001} planes 3:1 and 1:3 stoichiometries of Bi and Na are realized. Space groups of the configurations are given in Table 1. '111' and 'all3+1' cation arrangements lead to cubic symmetry, while the remaining configurations result in tetragonal systems.

For clarity, we first present the effects of different A-cation configurations on stability and local structure in the high-temperature cubic cell symmetry and then analyze the chemical origin.

3. Results and discussion

3.1. Relative stability

We calculated total energies of the different Bi/Na-orders in ideal cubic perovskite structures and in relaxed structures, the results are

shown in Fig. 3 (contributions from ionic and cell shape relaxation are given separately). In the ideal perovskites the different configurations reveal only small variations in total energy of less than 120 meV, with '110' being the most favored and '001' being the most unfavored order type. Taking structural relaxations into account the maximal difference is almost doubled (220 meV). The most stable structure now is the layered '001' configuration, while the rock salt ordered system '111' becomes the most unfavored one. We find that the more unstable a structure is in the ideal perovskite the more energy it can gain from structural relaxation. The rock salt ordered system does not show any structural relaxation, while all other structures can gain reasonable amounts of energy up to 300 meV. This is demonstrated in Fig. 4, where the correlation between DFT relaxation energies and Coulomb lattice sums of the different cation configurations on the ideal perovskite lattice (blue) is shown. The smaller the ionic contribution to the total energy, the larger is the energy gain by local atomic relaxation. Additionally, we show the correlation between DFT total energies and Coulomb energies (green). This correlation is rather poor, indicating that ionic interactions play a minor role and electronic interactions might be more important in this material as commonly assumed.

3.2. Structural relaxation

In the following we want to investigate the structural changes and stabilizing factors responsible for the high relaxation energies in the '001', '10-01_z' and 'all3+1' configurations and the much lower relative stability of the rock salt ordered structure.

As discussed before, the existence and type of ionic order is determined by the interplay of charge, size and bonding effects. From the electrostatic point of view rock salt order of the Na⁺ and Bi³⁺ ions with alternating layers along the <111>-directions should be the ground state structure of the simple cubic A-site sublattice in NBT, as can be seen from the order of Coulomb lattice sums of the different configurations given in Fig. 4. On the other hand, the ionic radii of bismuth and sodium are almost the same: Bi 1.45 Å and Na 1.39 Å [38], but the Bi³⁺ ion size depends, however, strongly on the degree of the 6s² lone pair character. Both ions differ strongly in their bonding properties though, Na forms exclusively ionic bonds while Bi can also contribute covalent bonding parts. Closely related to these cationic properties is the displacing ability of the anionic perovskite sublattice.

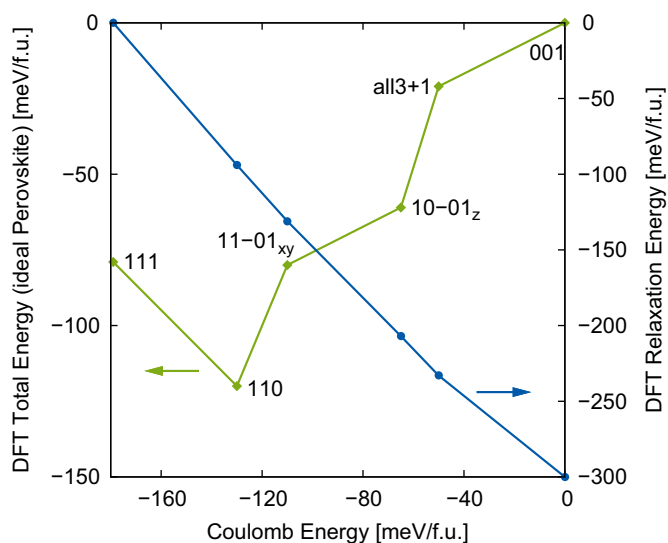


Fig. 4. Correlation between DFT total energies and Coulomb energies (with $\epsilon_r = 10$) of different cation configurations on the ideal perovskite lattice (green) and between DFT relaxation energies and Coulomb energies (blue). The higher the Coulomb energy of the cation configuration the more energy can the system gain from local structural relaxation. (For interpretation of the references to color in this figure legend, the reader is referred to the web version of this article.)

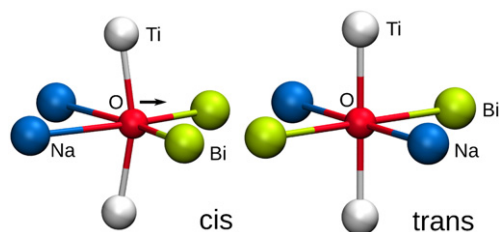


Fig. 5. Oxygen environments in the $2 \times \text{Bi}/2 \times \text{Na}$ (cis)- and $2 \times \text{Bi}/2 \times \text{Na}$ (trans)-coordination. The cis-coordination allows relaxation of the oxygen anion while the trans-coordination does not.

In the perovskite structure oxygen is quasi-octahedrally coordinated by Bi/Na- and Ti-atoms, with two Ti-atoms in the axial positions of the octahedron at a distance of $a/2$ and four Bi/Na-atoms in the equatorial positions at a distance of $a/\sqrt{2}$, resulting in six possible oxygen environments characterized by the Bi/Na-coordination: $4 \times \text{Na}$, $4 \times \text{Bi}$, $1 \times \text{Bi}/3 \times \text{Na}$, $3 \times \text{Bi}/1 \times \text{Na}$, and $2 \times \text{Bi}/2 \times \text{Na}$ in cis- or trans-coordination, the latter two are shown in Fig. 5. An oxygen ion is expected to displace, if there are significant differences in size, charge or bond strength of the coordinating cations and if the oxygen ion is not an inversion center. Hence, among the six possible coordinations, there are three where no displacement of the oxygen ion is possible (inversion symmetry), namely $4 \times \text{Na}$, $4 \times \text{Bi}$ and $2 \times \text{Bi}/2 \times \text{Na}$ (trans), one coordination where displacing is severely facilitated $2 \times \text{Bi}/2 \times \text{Na}$ (cis), while in $3 \times \text{Bi}/1 \times \text{Na}$ and $1 \times \text{Bi}/3 \times \text{Na}$ smaller displacements towards the Bi ions can occur. These displacements can help to release local stresses and to compensate local charge imbalances, thus stabilizing certain configurations.

In Table 1 properties of the relaxed structures like c/a -ratio and maximum displacements of Ti and O (Bi/Na do not displace from their ideal positions) are summarized. According to the space group symmetries of some A-cation configurations cell shapes may become tetragonal, but c/a -ratios are close to 1.000. We see that the Ti-cations are not considerably displaced. Only oxygen anions show significant displacements from their ideal positions. Also given are occurrences of the different oxygen coordinations

regarding Bi/Na. All possible oxygen coordinations mentioned above can be found in the six supercell-configurations. $4 \times \text{Na}$ and $4 \times \text{Bi}$ coordinations are only present in the '001' configuration, but $2 \times \text{Bi}/2 \times \text{Na}$ (trans) is present in several configurations, namely the three with the lowest energy gain from relaxation: '111', '110' and '11-01_{xy}'. Oxygen ions in these three coordinations do not displace from their ideal positions, as expected. The '001' configuration shows the highest relaxation energy and the majority of oxygen anions can be found in the $2 \times \text{Bi}/2 \times \text{Na}$ (cis) coordination, where oxygen anions are displaced from their ideal position towards the higher charged and stronger bonding bismuth ions as shown in Fig. 5, resulting in size-decreased Bi-polyhedra and size-increased Na-polyhedra, e.g. in the '001' configuration Bi-O distances are decreased from 2.77 Å in the ideal structure to 2.66 Å in the locally relaxed structure. The 3+1 coordinated oxygen ions also displace toward the bismuth ions.

In summary, local ionic displacements are observed mainly on the oxygen sublattice in the exact way postulated by Woodward [25,26], while almost no displacements on the two cation sublattices are observed. Moreover, structural relaxation can reverse the stability of the considered configurations with respect to the ideal perovskite structure. In the rock salt ordered structure all oxygen anions are in the $2 \times \text{Bi}/2 \times \text{Na}$ (trans) coordination, which explains why this configuration does not relax at all.

In Table 1 also the bandgaps of the relaxed structures are given; they are in the range of 1.50–2.01 eV. Experiments revealed an indirect optical bandgap of 3.20–3.30 eV in thin films [39]. It is well known that LDA underestimates bandgaps by up to 100%, but comparison of bandgaps of the same compound only differing in the cation configuration should not be affected by this. We find that local ionic displacements increase the bandgaps, the rock salt structure has the smallest bandgap which is 0.5 eV below the highest value found in the '10-01_z' configuration.

3.3. Density of states

In Fig. 6 we show total and site-, l - and m_l -projected densities of states of the '111' and the '001' configurations in ideal perovskite (black dotted line) and structurally relaxed structures (filled). In the '111' configuration only one type of oxygen is present, $2 \times \text{Bi}/2 \times \text{Na}$ (trans), while in the '001' configuration we have three different oxygen atoms: $4 \times \text{Na}$, $4 \times \text{Bi}$ and $2 \times \text{Bi}/2 \times \text{Na}$ (cis) (cf. Table 1). There are also two different types of Bi 6p-orbitals, two lying in the Bi-layer and one perpendicular to it pointing towards the neighboring Na-layer. All configurations show a bandgap of 1.50–2.01 eV. The conduction band is formed dominantly by Bi 6p-states and Ti 3d-states, which split in the octahedral crystal field into t_{2g} -states on the lower energy part of the conduction band and e_g -states, which again split into bonding (in the valence band at -4.5 eV) and anti-bonding (the upper conduction band part above 4.0 eV) states due to interaction with the O 2p-states. The valence band is formed dominantly by O 2p-states, with small contributions from Ti 3d- and Bi 6sp-states. The maximum of the Bi 6s-states lies deep below the valence band at -10.0 eV (not shown). The O 2p-states differ depending on m_l and Bi/Na-coordination of the particular oxygen atom, those orbitals pointing towards Ti show two maxima at the bottom and the top of the valence band, while those orbitals pointing towards Bi/Na show a big maximum only in the upper part of the valence band.

There are three differences between the ideal and relaxed structures' DOS.

- Local oxygen displacements increase the bandgap. The conduction band states are shifted to higher energies by about 0.3 eV in the '001' configuration.

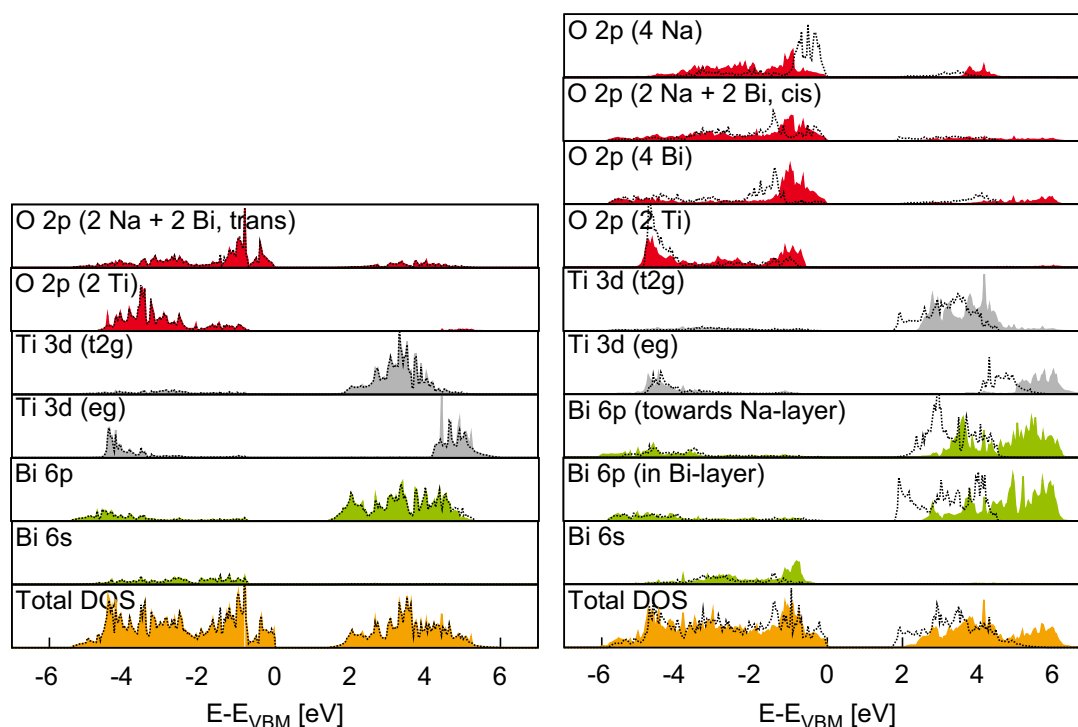


Fig. 6. Densities of states of configurations '111' (left) and '001' (right) before (black dotted line) and after relaxation (filled). Energies are given relative to the valence band maximum. On structural relaxation—possible in all structures besides the '111' configuration—band gaps are enlarged and changes especially of the Bi 6s- and O 2p-state densities occur.

- The order of oxygen states at the valence band maximum changes. In the ideal perovskite structure the VBM is formed dominantly by oxygen ions with Na-excess, while oxygen ions with Bi-excess have their density maximum below 0.7 eV. Orbitals with sodium excess are lowered while orbitals with bismuth excess are lifted in energy. These shifts reflect the energy shifts of the coordinating A-cations. The lower lying semi-core states Bi 5*d* and Na 2*p* (not shown) are shifted by +1.0 and −0.5 eV, respectively, showing that the on-site Madelung potential of Bi is more favorable in the relaxed structure with local oxygen displacements while that for Na is less favorable.
- Additional Bi 6*s*-states arise at the top of the valence band. Although the maximum of 6*s*-states stays below the valence band around −10.0 eV, there is a significant increase in the state density in the anti-bonding region above −2 eV, these states mix with both the Bi 6*p*-states and the O 2*p*-states, which is characteristic for the formation of a stereochemically active Bi³⁺ lone pair [40].

3.4. Chemical ordering

Generally, chemical ordering will occur if there is a decisive energy difference between a most favored ordered configuration and other structures and if this energy difference is higher than the entropy contribution of mixing.

We find an energy difference of 34 meV between the two most stable structures '001' and '10-01_z'. The entropy contribution of mixing to the free energy in the disordered state can be approximated by the configurational entropy of an ideal solution with $x_{\text{Bi}} = x_{\text{Na}} = 0.5$

$$-T\Delta S = -k_B T[-x_{\text{Bi}} \ln x_{\text{Bi}} - x_{\text{Na}} \ln x_{\text{Na}}]$$

This approximation gives a lower limit for the ordering temperature, since the ideal solution model is overestimating the mixing

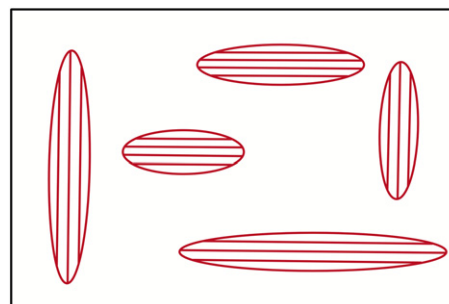


Fig. 7. Structure model for NBT: Chemically 001-ordered nano-regions embedded in a disordered matrix.

entropy. At sintering conditions the energy equivalent $T\Delta S$ is more than twice the obtained energy difference between the most stable ordered states, thus the disordered state is favored over all ordered states. The critical temperature is about 570 K. Chemical long-range ordering can therefore be ruled out, but short-range ordering with alternating layers of Bi and Na along $\langle 001 \rangle$ -directions is still possible to occur as schematically shown in Fig. 7. These small chemically ordered areas can act as nucleation sites for polar nano-regions, which would explain the relaxor behavior of NBT. Please note that alternating layers of different charges lead to depolarizing fields, which can have an impact on the polar properties of the low temperature phases.

4. Conclusions

We investigated structural and electronic properties of NBT depending on Bi/Na-order in supercells containing 40 atoms by total energy calculations based on density functional theory. The importance of structural relaxation in the ordered states is shown

and the driving force for this process identified. Most energy is gained by hybridization of Bi 6*s*–*p* states. This hybridization leading to stereochemically active Bi³⁺ lone pairs increases the stability especially of structures with layers of high Bi-concentrations in {001}-planes. This kind of planes was considered by Kreisel et al. to explain the diffuse scattering patterns indicative for Guinier-Preston-Zones [15]. However, comparison of total energy differences between the ordered structures and entropy of mixing of the disordered state assuming an ideal solution shows that at temperatures higher than 570 K chemical ordering is unlikely, but different degrees of short-range order can occur depending on synthesis conditions. We report for the first time on displacive disorder on the oxygen sublattice, which up to now has been neglected in experimental studies and should be investigated in more detail in future research. A comprehensive investigation of the local structures caused by different local chemical configurations in the low temperature phases has to follow as NBT combines long-range polar shifts along different directions and both in- and out-of-phase oxygen octahedral tilts offering a rich playground to investigate coupling/competing between all these different degrees of freedom.

Acknowledgments

This work has been financially supported by the LOEWE-Center “Adaptronics—Research, Innovation, Application” and by the DFG Center of Excellence 595 “Electrical Fatigue in Functional Materials”. Moreover, this work was made possible by grants for computing time on supercomputers at HRZ Darmstadt.

References

- [1] Y. Hiruma, H. Nagata, T. Takenaka, *Journal of Applied Physics* 105 (2009) 084112.
- [2] H. Nagata, *Journal of the Ceramic Society of Japan* 116 (2008) 271–277.
- [3] W. Jo, T. Granzow, E. Aulbach, J. Rödel, D. Damjanovic, *Journal of Applied Physics* 105 (2009) 094102.
- [4] G.A. Smolenskii, V.A. Isupov, A.I. Agranovskaya, S.N. Popov, *Soviet Physics—Solid State* (1961) 2584–2594.
- [5] G.O. Jones, P.A. Thomas, *Acta Crystallographica Section B—Structural Science* 56 (2000) 426–430.
- [6] G.O. Jones, P.A. Thomas, *Acta Crystallographica Section B—Structural Science* 58 (2002) 168–178.
- [7] S. Gorfman, P.A. Thomas, *Journal of Applied Crystallography* 43 (2010) 1409–1414.
- [8] P.A. Thomas, J. Kreisel, A.M. Glazer, P. Bouvier, Q.Z. Jiang, R. Smith, *Zeitschrift fuer Kristallographie* 220 (2005) 717–725.
- [9] V. Dorcet, G. Trolliard, P. Boullay, *Chemistry of Materials* 20 (2008) 5061–5073.
- [10] G. Trolliard, V. Dorcet, *Chemistry of Materials* 20 (2008) 5074–5082.
- [11] K. Sakata, Y. Masuda, *Ferroelectrics* 7 (1974) 347–349.
- [12] J.E. Daniels, W. Jo, J. Rödel, J.L. Jones, *Applied Physics Letters* 95 (2009).
- [13] S.E. Park, S.J. Chung, I.T. Kim, K.S. Hong, *Journal of the American Ceramic Society* 77 (1994) 2641–2647.
- [14] J. Petzelt, S. Kamba, J. Fabry, D. Noujmi, V. Porokhonskyy, A. Pashkin, I. Franke, K. Roleder, J. Suchanicz, R. Klein, G.E. Kugel, *Journal of Physics—Condensed Matter* 16 (2004) 2719–2731.
- [15] J. Kreisel, P. Bouvier, B. Dkhil, P.A. Thomas, A.M. Glazer, T.R. Welberry, B. Chaabane, M. Mezouar, *Physical Review B* 68 (2003) 014113.
- [16] P.A. Thomas, S. Trujillo, M. Boudard, S. Gorfman, J. Kreisel, *Solid State Sciences* 12 (2010) 311–317.
- [17] V.A. Shuvaeva, D. Zekria, A.M. Glazer, Q. Jiang, S.M. Weber, P. Bhattacharya, P.A. Thomas, *Physical Review B* 71 (2005) 174114.
- [18] Y.N. Xu, W.Y. Ching, *Philosophical Magazine B—Physics of Condensed Matter Statistical Mechanics Electronic Optical and Magnetic Properties* 80 (2000) 1141–1151.
- [19] B.P. Burton, E. Cockayne, *Fundamental Physics of Ferroelectrics* 2001 582 (2001) 82–90.
- [20] J. Kling, S. Hayn, L.A. Schmitt, M. Gröting, H.J. Kleebe, K. Albe, *Journal of Applied Physics* 107 (2010).
- [21] J. Rödel, W. Jo, K.T.P. Seifert, E.M. Anton, T. Granzow, D. Damjanovic, *Journal of the American Ceramic Society* 92 (2009) 1153–1177.
- [22] L.E. Cross, *Ferroelectrics* 76 (1987) 241–267.
- [23] A.A. Bokov, Z.G. Ye, *Journal of Materials Science* 41 (2006) 31–52.
- [24] P.K. Davies, H. Wu, A.Y. Borisevich, I.E. Molodetsky, L. Farber, *Annual Review of Materials Research* 38 (2008) 369–401.
- [25] M.C. Knapp, P.M. Woodward, *Journal of Solid State Chemistry* 179 (2006) 1076–1085.
- [26] G. King, P.M. Woodward, *Journal of Materials Chemistry* 20 (2010) 5785–5796.
- [27] P. Hohenberg, W. Kohn, *Physical Review* 136 (1964) B864–B871.
- [28] W. Kohn, L.J. Sham, *Physical Review* 140 (1965) 1133.
- [29] G. Kresse, J. Hafner, *Physical Review B* 47 (1993) 558–561.
- [30] G. Kresse, J. Hafner, *Physical Review B* 49 (1994) 14251–14269.
- [31] G. Kresse, J. Furthmüller, *Computational Materials Science* 6 (1996) 15–50.
- [32] G. Kresse, J. Furthmüller, *Physical Review B* 54 (1996) 11169–11186.
- [33] G. Kresse, D. Joubert, *Physical Review B* 59 (1999) 1758–1775.
- [34] P.E. Blöchl, *Physical Review B* 50 (1994) 17953–17979.
- [35] D.M. Ceperley, B.J. Alder, *Physical Review Letters* 45 (1980) 566–569.
- [36] H.J. Monkhorst, J.D. Pack, *Physical Review B* 13 (1976) 5188–5192.
- [37] J.P. Perdew, A. Zunger, *Physical Review B* 23 (1981) 5048–5079.
- [38] R.D. Shannon, *Acta Crystallographica Section A* 32 (1976) 751–767.
- [39] M. Bousquet, J.R. Duclere, E. Orhan, A. Bouille, C. Bachelet, C. Champeaux, *Journal of Applied Physics* 107 (2010) 104107.
- [40] L.A. Olsen, J. Lopez-Solano, A. Garcia, T. Balic-Zunic, E. Makovicky, *Journal of Solid State Chemistry* 183 (2010) 2133–2143.